The Role of Oceanic Heat Advection in the Evolution of Tropical North and South Atlantic SST Anomalies*

GREGORY R. FOLTZ AND MICHAEL J. MCPHADEN

NOAA/Pacific Marine Environmental Laboratory, Seattle, Washington

(Manuscript received 21 November 2005, in final form 7 April 2006)

ABSTRACT

The role of horizontal oceanic heat advection in the generation of tropical North and South Atlantic sea surface temperature (SST) anomalies is investigated through an analysis of the oceanic mixed layer heat balance. It is found that SST anomalies poleward of 10° are driven primarily by a combination of wind-induced latent heat loss and shortwave radiation. Away from the eastern boundary, horizontal advection damps surface flux–forced SST anomalies due to a combination of mean meridional Ekman currents acting on anomalous meridional SST gradients, and anomalous meridional currents acting on the mean meridional SST gradient. Horizontal advection is likely to have the most significant effect on the interhemispheric SST gradient mode through its impact in the 10°–20° latitude bands of each hemisphere, where the variability in advection is strongest and its negative correlation with the surface heat flux is highest. In addition to the damping effect of horizontal advection in these latitude bands, evidence for coupled wind–SST feedbacks is found, with anomalous equatorward (poleward) SST gradients contributing to enhanced (reduced) westward surface winds and an equatorward propagation of SST anomalies.

1. Introduction

In contrast to the ENSO-dominated SST variability in the tropical Pacific, SST variability in the tropical Atlantic on seasonal-to-decadal time scales involves two distinct modes. The first mode is similar to ENSO and is associated with anomalous SST in the eastern equatorial Atlantic, a weakening of the trade winds in the central basin, and a southward shift of convection in the intertropical convergence zone (ITCZ; Carton and Huang 1994; Ruiz-Barradas et al. 2000). The second mode, which does not have a strong counterpart in the tropical Pacific, is characterized by an anomalous meridional SST gradient centered near the equator, with anomalous SST signals extending into the subtropical North and South Atlantic (Servain 1991; Nobre and Shukla 1996; Huang et al. 2004). This mode is associated with anomalous cross-equatorial surface winds and a meridional displacement of the ITCZ. An anomalous northward SST gradient is associated with anomalous northward cross-equatorial winds, a northward displacement of the ITCZ, reduced rainfall in Northeast Brazil, and enhanced rainfall in sub-Saharan Africa (Lamb 1978; Hastenrath and Greischar 1993; Nobre and Shukla 1996).

Previous studies have suggested that oscillations of the gradient mode are caused by a combination of direct atmospheric forcing, coupled wind–evaporation–SST feedback, and horizontal oceanic heat advection (Carton et al. 1996; Chang et al. 2001; Czaja et al. 2002). The role of oceanic heat advection in the development of off-equatorial SST anomalies remains uncertain despite having been the focus of several recent modeling studies. Xie (1999) used a simple coupled model with a slab oceanic mixed layer to predict that meridional Ekman advection will damp off-equatorial SST anomalies in the tropical Atlantic. Chang et al. (2001) hypothesized that oscillations of the anomalous interhemispheric SST gradient in the tropical Atlantic are driven by an imbalance between positive ocean–atmosphere feedback and negative oceanic heat advection feedback in the tropical North Atlantic, with surface fluxes leading horizontal advection by ~2 yr. In contrast, Seager et

* Pacific Marine Environmental Laboratory Contribution Number 2914.

Corresponding author address: Gregory R. Foltz, NOAA/Pacific Marine Environmental Laboratory, 7600 Sand Point Way NE, Seattle, WA 98115.
E-mail: gregory.foltz@noaa.gov

al. (2001) found no evidence of a significant phase lag between surface fluxes and horizontal advection, suggesting that the role of oceanic heat advection is simply to damp the surface flux–forced SST anomalies. They also showed that horizontal heat advection is strongest within 10° of the equator, where the mean Ekman currents are the strongest. Both Chang et al. (2001) and Seager et al. (2001) found that the dominant component of the heat advection term is the mean meridional currents acting on anomalous SST gradients. Joyce et al. (2004) showed that anomalous wind stress curl associated with the gradient mode forces anomalous cross-equatorial oceanic heat transport with a lag of a few months, damping the existing anomalous SST gradient. Their results suggest that the action of anomalous wind-forced meridional currents on the mean meridional SST gradient may play an important role in the evolution of the gradient mode.

In this study we use a combination of satellite and atmospheric reanalysis data to examine the role of horizontal oceanic heat advection in the evolution of SST anomalies in the tropical North and South Atlantic. We focus on the region poleward of 5° of latitude, where currents can be estimated diagnostically from available surface wind and sea level datasets.

2. Data

Surface latent and sensible heat fluxes are obtained from a combination of satellite and reanalysis products on a 1° × 1° grid for the time period 1981–2002 (Yu et al. 2004). The reanalysis products consist of the National Centers for Environmental Prediction–Department of Energy (NCEP–DOE) reanalysis 2 (hereafter NCEP2 reanalysis; Kanamitsu et al. 2002) and the European Centre for Medium-Range Weather Forecasts (ECMWF) 40-yr reanalysis (Simmons and Gibson 2000). Surface turbulent fluxes were computed from these products using daily mean wind speed, SST, and humidity in the bulk flux algorithm developed from the Coupled Ocean–Atmosphere Response Experiment (COARE; Fairall et al. 2003) and are an improvement over the turbulent fluxes from atmospheric reanalyses (Yu et al. 2004). Surface shortwave radiation is obtained from the satellite-based dataset of Zhang et al. (2004), which is available during 1983–2004 on a 2.5° × 2.5° × monthly grid. Surface longwave radiation is obtained from the NCEP2 reanalysis on a 2° × 2° × daily grid for the time period 1979–2004. We also use the Yu et al. (2004) wind speed and specific humidity, along with weekly Reynolds et al. (2002) SST, to estimate separately the wind speed and humidity contributions to the latent heat flux.

To estimate mixed layer heat storage, we use Reynolds et al. (2002) SST together with the monthly mean climatological mixed layer depths from de Boyer Montégut et al. (2004), available on a 2° × 2° grid, and from the World Ocean Database, available on a 1° × 1° grid (Monterey and Levitus 1997). These SST and mixed layer depth datasets are also used in conjunction with NCEP2 reanalysis wind velocity to estimate horizontal mixed layer Ekman heat advection.

To estimate geostrophic currents, we have obtained ERS-1/2/TOPEX/Poseidon/Jason altimeter sea level anomaly data for the time period 1992–2002 from the Collect Localisation Satellites (CLS) Space Oceanography Division. The anomalies are referenced to the 1993–99 mean and are mapped according to the methodology of Ducet et al. (2000). The data are available every 7 days on a ⅓° × ⅓° grid. We have added the 1993–99 mean dynamic topography (Rio and Hernandez 2004) to the sea level anomaly data in order to estimate the total geostrophic surface currents. We have converted each of the aforementioned datasets from its original resolution to a 2° × 2° × monthly grid for consistent analysis across all fields.

3. Methodology

To examine the role of horizontal advection in the evolution of tropical Atlantic SST anomalies, we consider the mixed layer heat balance, which can be written

$$h\frac{\partial T}{\partial t} = -h\mathbf{v}\cdot\nabla T - H\Delta T w_e - \nabla\cdot\int_{-h}^{0}\hat{\mathbf{v}}\hat{T}\,dz + \frac{q_0 - q_{-h}}{\rho c_p}, \qquad (1)$$

following Moisan and Niiler (1998). The terms represent, from left to right, local storage, horizontal advection, entrainment, vertical temperature/velocity covariance, net surface heat flux adjusted for the penetration of light below the mixed layer (q_0), and vertical turbulent diffusion at the base of the mixed layer (q_{-h}). Here h is the depth of the mixed layer; T and υ are temperature and velocity, respectively, vertically averaged from the surface to a depth of $-h$; $\hat{T}$ and $\hat{\mathbf{v}}$ are deviations from the vertical average; H is the Heavyside unit function, $\Delta T = T - T_{-h}$; and w_e is entrainment velocity. We neglect entrainment, the vertical temperature difference/velocity shear covariance term, and q_{-h} since we cannot reliably estimate them. The results of Carton et al. (1996) and Foltz et al. (2003) indicate that these terms are likely of minor importance in comparison to surface fluxes in the tropical North and South Atlantic.

For all terms in (1) we form anomalies by removing the monthly mean seasonal cycle and then smooth with

a 5-month running mean to emphasize variability on interannual and longer time scales.

The mixed layer depth, h, which contributes to the storage and advection terms in (1), is affected by the vertical distributions of both temperature and salinity. We therefore use the density-based climatological mixed layer depth estimates of de Boyer Montégut et al. (2004), which are based on individual temperature and salinity profiles and are defined using the criterion of a 0.03 kg m^{-3} density increase from a depth of 10 m. We fill data gaps with the mixed layer depth estimates of Monterey and Levitus (1997). These estimates are based on gridded temperature and salinity profiles from the World Ocean Database, with gaps filled by the longitudinal mean temperature and salinity within the tropical Atlantic, and are defined using the criterion of a 0.125 kg m^{-3} density increase from the surface. We have found that the two mixed layer depth climatologies agree reasonably well in the tropical North Atlantic (5°–20°N, 30°–60°W), where the data coverage is the best. The Monterey and Levitus (1997) h is shallower than the corresponding de Boyer Montégut et al. (2004) h during all months except April, with monthly differences of at most 30% of the Monterey and Levitus h (~5 m during April–December and 10–15 m during January–March). Since the data gaps are confined mainly to the region south of 10°S, we expect that our mixed layer depth estimates in this region contain a much higher degree of uncertainty than in the remainder of the tropical Atlantic.

We use the climatological mixed layer depth estimates since there are not enough in situ temperature and salinity measurements to produce reliable monthly mean estimates. We repeat the climatology for each year, thus eliminating interannual variations of mixed layer depth. The results of Carton et al. (1996) suggest that, away from the eastern boundary, interannual variations in mixed layer depth are unimportant in the off-equatorial heat balance.

The time rate of change of mixed layer temperature ($\partial T/\partial t$) is estimated using monthly Reynolds et al. (2002) SST. The results of Foltz and McPhaden (2005) indicate that SST is a good proxy for T in the tropical North Atlantic, and we anticipate a similarly good agreement in the tropical South Atlantic, where salinity contributes less to the near-surface stratification and hence the mixed layer depth (Sprintall and Tomczak 1992).

The surface heat flux consists of the latent and sensible heat fluxes (LHF and SHF, respectively), shortwave radiation absorbed in the mixed layer (SWR), and net longwave radiation (LWR) emitted from the sea surface. All surface fluxes are defined as positive when they act to heat the mixed layer. LHF and SHF are obtained from the Yu et al. (2004) dataset. SWR is obtained from the Zhang et al. (2004) dataset, and LWR is obtained from the NCEP2 reanalysis. Following Wang and McPhaden (1999), we model the amount of shortwave radiation penetrating the mixed layer as $Q_{\text{pen}} = 0.47Q_{\text{sfc}}\, e^{-0.04h}$, where Q_{sfc} is the surface shortwave radiation and h is the depth of the mixed layer.

To estimate horizontal mixed layer heat advection, we follow Lagerloef et al. (1999) in assuming that the mixed layer velocity satisfies a linear steady momentum balance

$$fh\hat{\mathbf{k}} \times \mathbf{v} = -gh\nabla\eta + \frac{\tau}{\rho} - r\mathbf{v}_{\mathbf{e}}, \tag{2}$$

where $\hat{\mathbf{k}}$ is the vertical unit vector, $\mathbf{v} \equiv \mathbf{v_g} + \mathbf{v_e}$ is the horizontal velocity averaged vertically in the mixed layer ($\mathbf{v_g}$ and $\mathbf{v_e}$ are the geostrophic and Ekman components, respectively), η is sea level, τ is wind stress, and r is a linear drag coefficient. Following Grodsky and Carton (2001) we assign $r = 2 \times 10^{-4}$ m s^{-1}. To estimate horizontal mixed layer temperature advection, the velocity estimates are multiplied by Reynolds et al. (2002) SST gradients, calculated as a centered difference over a distance of 4°.

In the following two sections, we use correlation analysis on the terms in (1) to isolate the mechanisms responsible for changes in mixed layer heat content. We estimate confidence intervals for the correlations using a 1000-sample bootstrap test (Wilks 1995). Each sample consists of a series of randomly chosen monthly anomalies, which is then smoothed with a 5-month running mean. A statement that two time series are significantly correlated means that the correlation coefficient is significant at the 10% level according to the above method.

4. Local heat balance

In this section we consider the role of surface fluxes in the tropical Atlantic mixed layer heat balance, focusing on the time period July 1983–December 2002, when all datasets are available. We begin with an examination of the annual mean SST, winds, and surface heat fluxes in the tropical Atlantic. SST reaches a maximum just north of the equator with a poleward decrease that is strongest in the eastern half of the basin (Fig. 1a). The mean surface winds converge over the warmest SST and are strongest in the western basin. Here the wind stress acquires a strong zonal component, in contrast to the predominantly meridional component of wind stress in the east (Fig. 1b). The regions

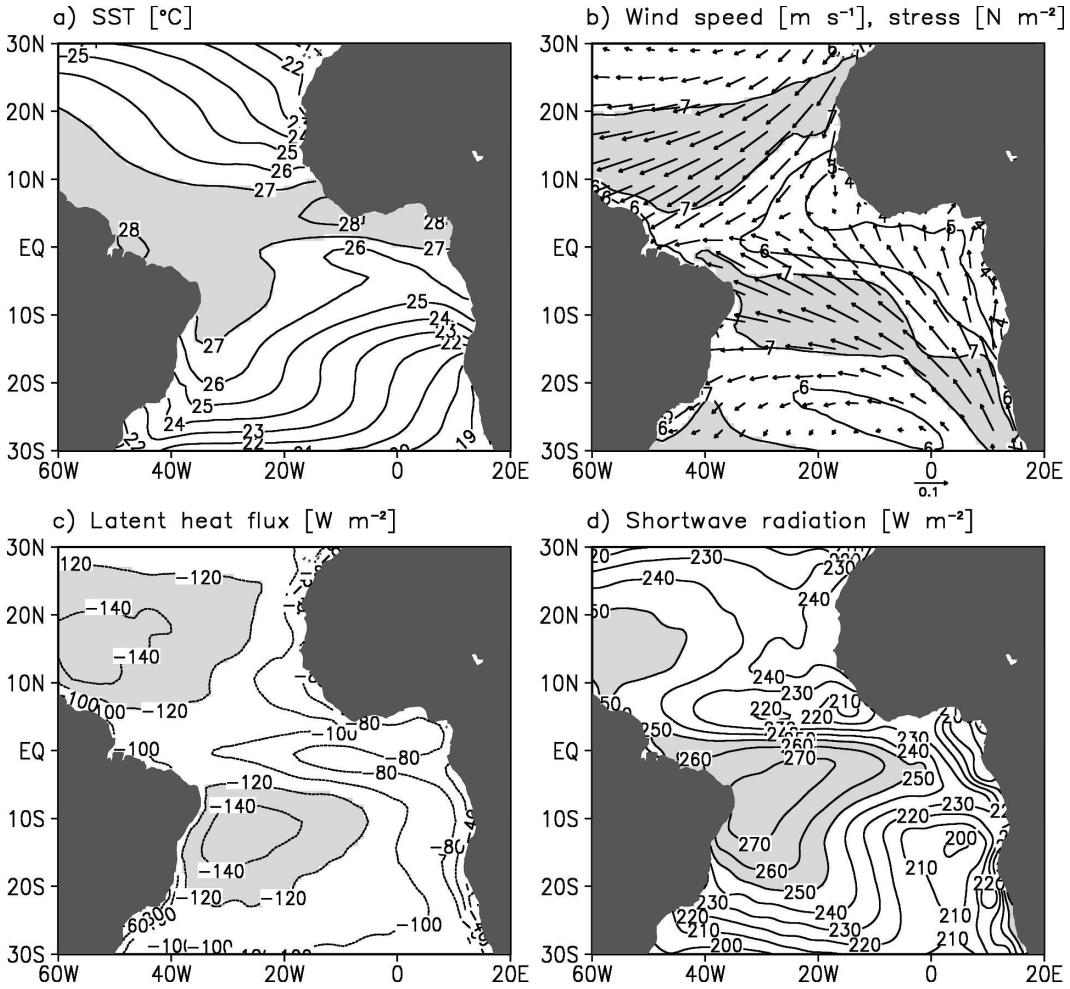

FIG. 1. Annual mean (1983–2002) (a) SST, (b) wind speed (contours) and stress (vectors), (c) latent heat flux (<0 indicates heat loss by the ocean), and (d) surface shortwave radiation (>0 indicates heat gain by the ocean). Shading emphasizes the regions where the magnitudes of annual mean values are largest.

of high wind speed and warm SST in the western basin generally coincide with the regions of maximum annual mean latent heat loss and surface shortwave radiation (Figs. 1c,d). The low values of shortwave radiation along the southwest coast of Africa reflect the presence of persistent low-level clouds (Klein and Hartmann 1993), while the local minimum in the 0°–10°N region is a consequence of cloudiness associated with the ITCZ.

Next, we consider the variability of SST and mixed-layer heat storage and the role of surface fluxes in forcing these changes. SST is organized into three regions of enhanced variability (standard deviation >0.4°C), located in the eastern tropical North Atlantic, the eastern equatorial region/Angolan coast, and the central tropical/subtropical South Atlantic (Fig. 2a). These areas were also identified by Huang et al. (2004) as related to the dominant spatial modes of SST variability in the tropical Atlantic. Since the annual mean mixed layer is very shallow in the eastern equatorial Atlantic (generally 10–30 m), the heat storage signal in this region is weak despite the strong SST variability (Fig. 2b). The mixed layer depth generally increases poleward and westward from the eastern equatorial zone, resulting in stronger storage variability in the northern and southern Tropics.

Previous studies have found that SST variability outside of ±10° of latitude is driven primarily by the LHF (Carton et al. 1996; Tanimoto and Xie 2002; Czaja et al. 2002). In agreement with these studies, we find that throughout most of the tropical Atlantic, LHF is the most important surface flux term in terms of both its magnitude and its correlation with local storage. The standard deviation of LHF exceeds 7 W m^{-2} in most of the basin, with the highest values in the tropical North Atlantic and the far eastern and western tropical South Atlantic (Fig. 3a). LHF is significantly positively corre-

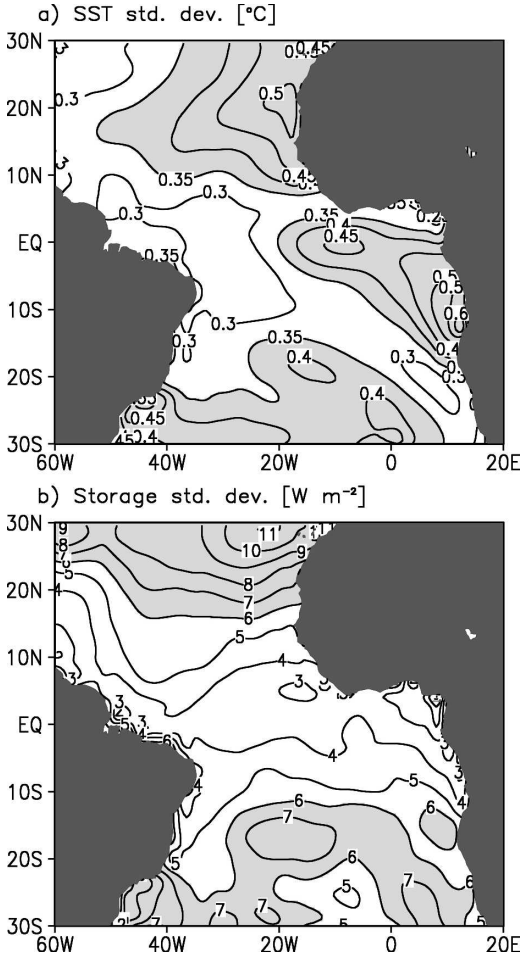

FIG. 2. Interannual standard deviations of (a) SST and (b) local mixed layer heat storage ($\rho c_p h \partial T/\partial t$), calculated from monthly anomalies from the seasonal cycle, smoothed with a 5-month running mean. Shading indicates regions of enhanced variability.

lated with local storage in the 10°–25° latitude band of each hemisphere (Fig. 3b), accounting for up to 30% of the variability in mixed layer heat storage.

In comparison to the LHF variability, SWR variability is weaker in the tropical North Atlantic and is more weakly correlated with local storage throughout the basin (Figs. 3c,d). SWR contributes most strongly along 10°S in the eastern basin, where its standard deviation approaches 10 W m^{-2} and its correlation with local storage is positive and significant. Another region of significant positive correlations extends from 10°N along the coast of South America northeastward into the subtropics.

Sensible heat flux and longwave radiation make relatively small contributions to the mixed layer heat balance in comparison to LHF and SWR, with standard deviations of <3 W m^{-2} throughout most of the tropical Atlantic. As a result, the total surface flux is due primarily to LHF and SWR. Its standard deviation peaks in the central equatorial Atlantic and along the boundaries of the tropical South Atlantic, where LHF variability is high (Fig. 3e). There is also a region of enhanced variability off the coast of Northwest Africa, where LHF and SWR variability are strong and positively correlated.

The total surface flux is significantly positively correlated with storage everywhere except in the 5°S–10°N latitude band, explaining a maximum of ~35% of the storage variance in the eastern tropical North and South Atlantic (Fig. 3f). The low values along the equator suggest an important role for oceanic heat advection in the mixed layer heat balance, in agreement with previous modeling studies (Carton et al. 1996). The net surface heat flux and local storage are significantly correlated in the tropical North Atlantic (10°–25°N, 20°–60°W) and in the tropical South Atlantic (5°–20°S, 30°W–10°E) (0.6 for the north, 0.7 for the south; Fig. 4). In both regions, the standard deviation of the surface flux exceeds that of the storage by ~40%, suggesting that other processes besides surface heat fluxes, such as horizontal heat advection and vertical entrainment/mixing, must be important in the mixed layer heat balance.

Since LHF is the most important flux term in the mixed layer heat balance, we next examine the causes of its variability by decomposing the terms in the bulk LHF expression:

$$\begin{aligned} \mathrm{LHF}' &= \rho_a L_e C_e [W'(\overline{q_s} - \overline{q}) + \overline{W}(q_s' - q')] \\ &= Q_w' + Q_q'. \end{aligned} \tag{3}$$

Here W is wind speed, q_s is saturation specific humidity at the sea surface, and q is specific humidity. The exchange coefficient (C_e) is estimated using the bulk flux algorithm of Fairall et al. (2003). Here the prime represents an anomaly from the mean seasonal cycle, smoothed with a 5-month running mean, and an overbar indicates the mean seasonal cycle. The terms in brackets represent the portions of the anomalous LHF due to variations of wind speed (Q_w') and the vertical humidity gradient (Q_q'). Nonlinear effects, which include terms with a product of two or more primed variables, are small in comparison to the terms in (3) and are therefore neglected.

Changes in LHF due to wind speed (Q_w') are strongest in the western basin in the latitude bands 10°–30°N and 10°–20°S (Fig. 5a), generally coinciding with the regions of strongest mean wind speed (Fig. lb). The Q_w' term is significantly correlated with LHF′ over most of

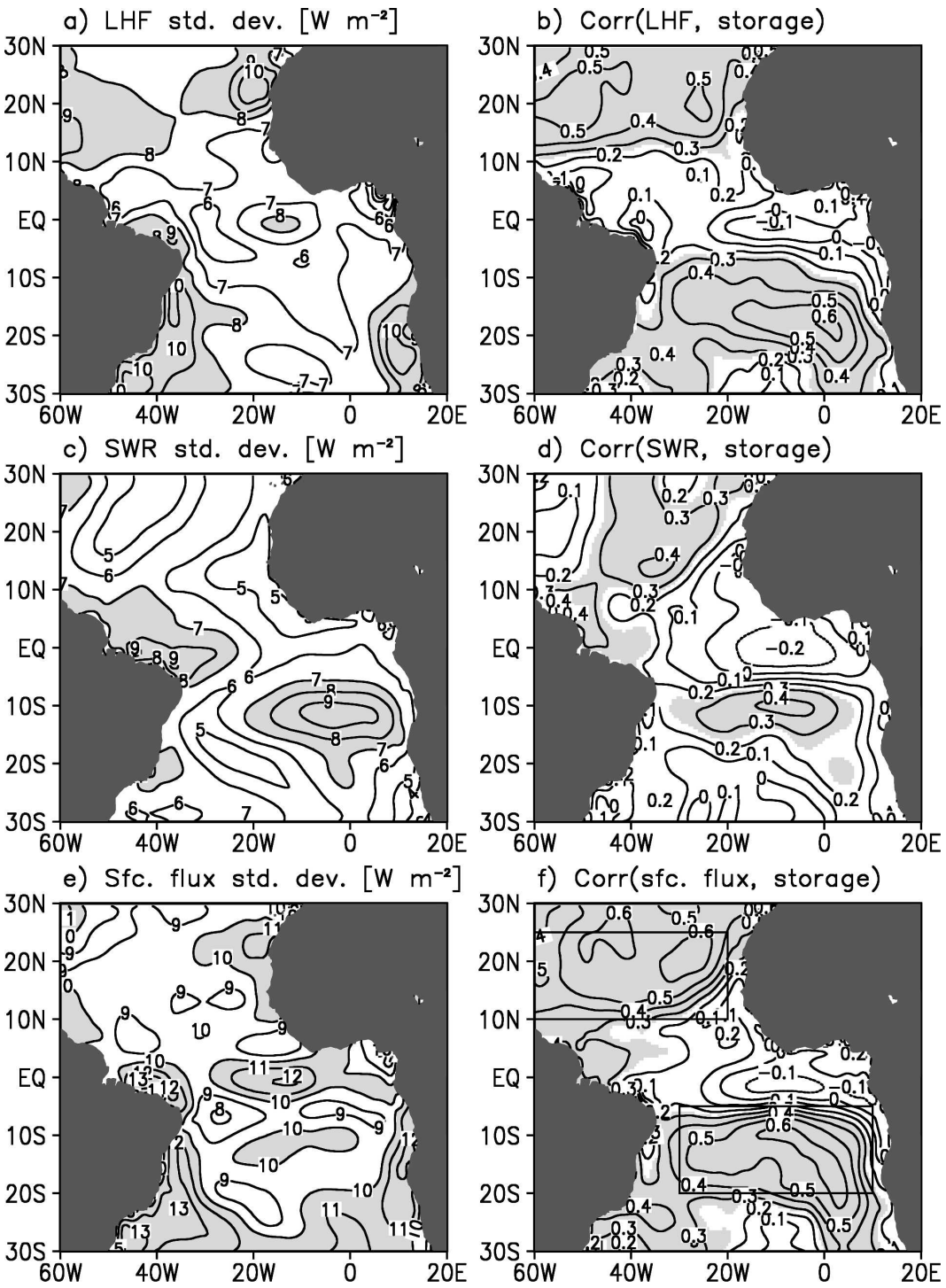

FIG. 3. (left) Interannual standard deviation of (a) LHF, (c) SWR, and (e) net surface flux (LHF + SWR + longwave + sensible). (right) Correlation of mixed layer heat storage ($h\partial T/\partial t$) with (b) LHF, (d) SWR, and (f) net surface heat flux. Shading in (a), (c), and (e) indicates regions of enhanced variability. Shading in (b), (d), and (f) indicates where the correlation is significant at the 10% level. Boxes in (f) enclose the regions used for averaging the net surface flux and storage shown in Fig. 4.

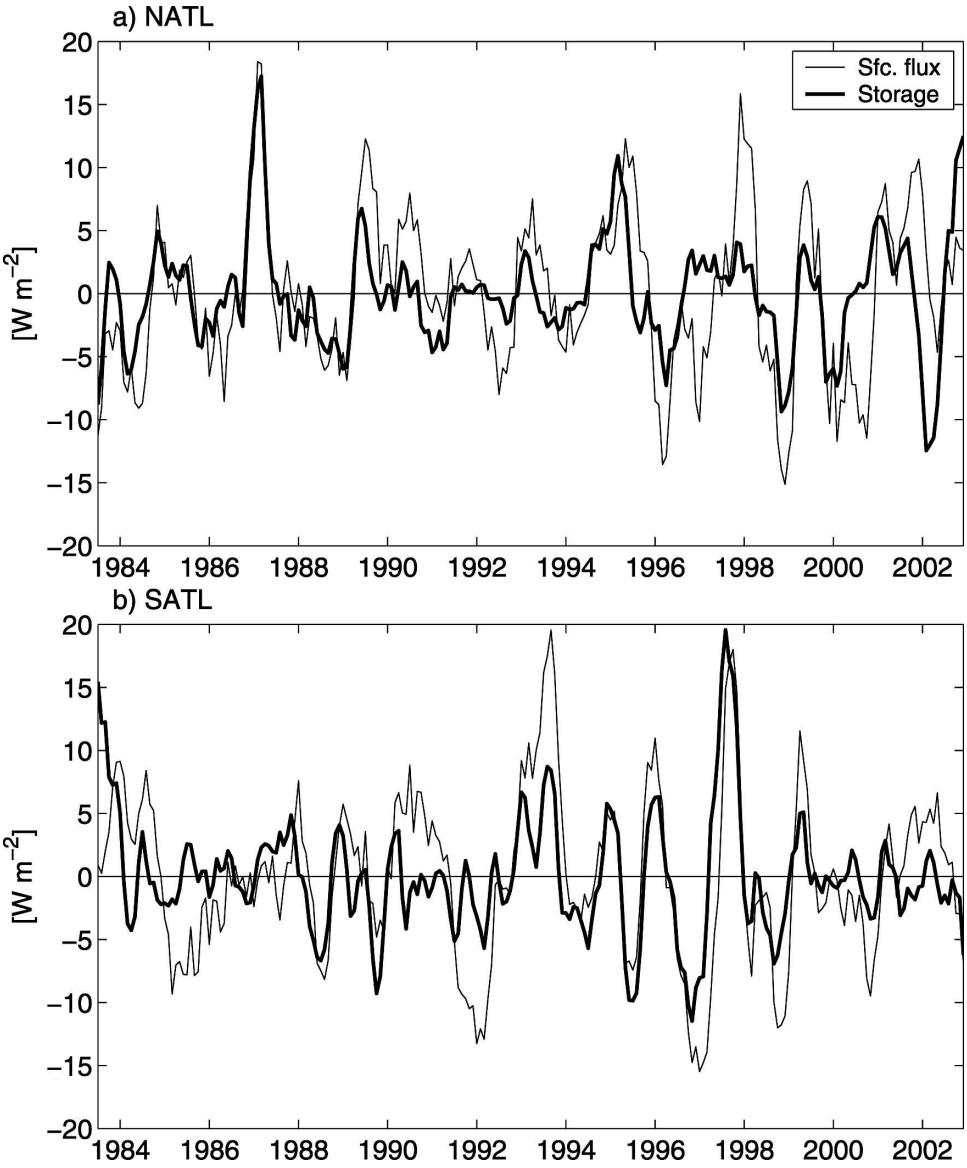

FIG. 4. Interannual anomalies of (a) net surface heat flux (thin) and mixed layer heat storage (thick) averaged in the tropical North Atlantic (10°–25°N, 20°–60°W). (b) Same as in (a), except for the tropical South Atlantic Atlantic (5°–20°S, 30°W–10°E; see Fig. 3f for the averaging regions).

the tropical Atlantic (Fig. 5b), with the highest correlations along 5°N in the central basin. Here changes in wind speed account for more than 60% of the LHF variability.

Over most the tropical North Atlantic, Q'_q is slightly weaker than Q'_w, while in the tropical South Atlantic, Q'_q is comparable to or stronger than Q'_w (Fig. 5c). Throughout most of the basin, changes in SST exert a much stronger influence on Q'_q than do changes in specific humidity. Correlations between SST' and Q'_q are positive and significant throughout most of the tropical Atlantic, whereas correlations between q' and Q'_q are mostly insignificant (Figs. 5e,f). The exceptions are along the coast of Namibia (20°–30°S) and in the northwestern basin (north of 20°N), where q' is significantly negatively correlated with Q'_q, and the correlations between SST' and Q'_q are weak. The results in the northwestern basin are consistent with Chikamoto and Tanimoto (2005), who found that ENSO-forced changes in humidity drive anomalous LHF over the northwestern tropical Atlantic Ocean and Caribbean Sea.

The correlation of Q'_q with LHF$'$ is generally highest where the SST variability is strongest (Figs. 2a, 5d) and

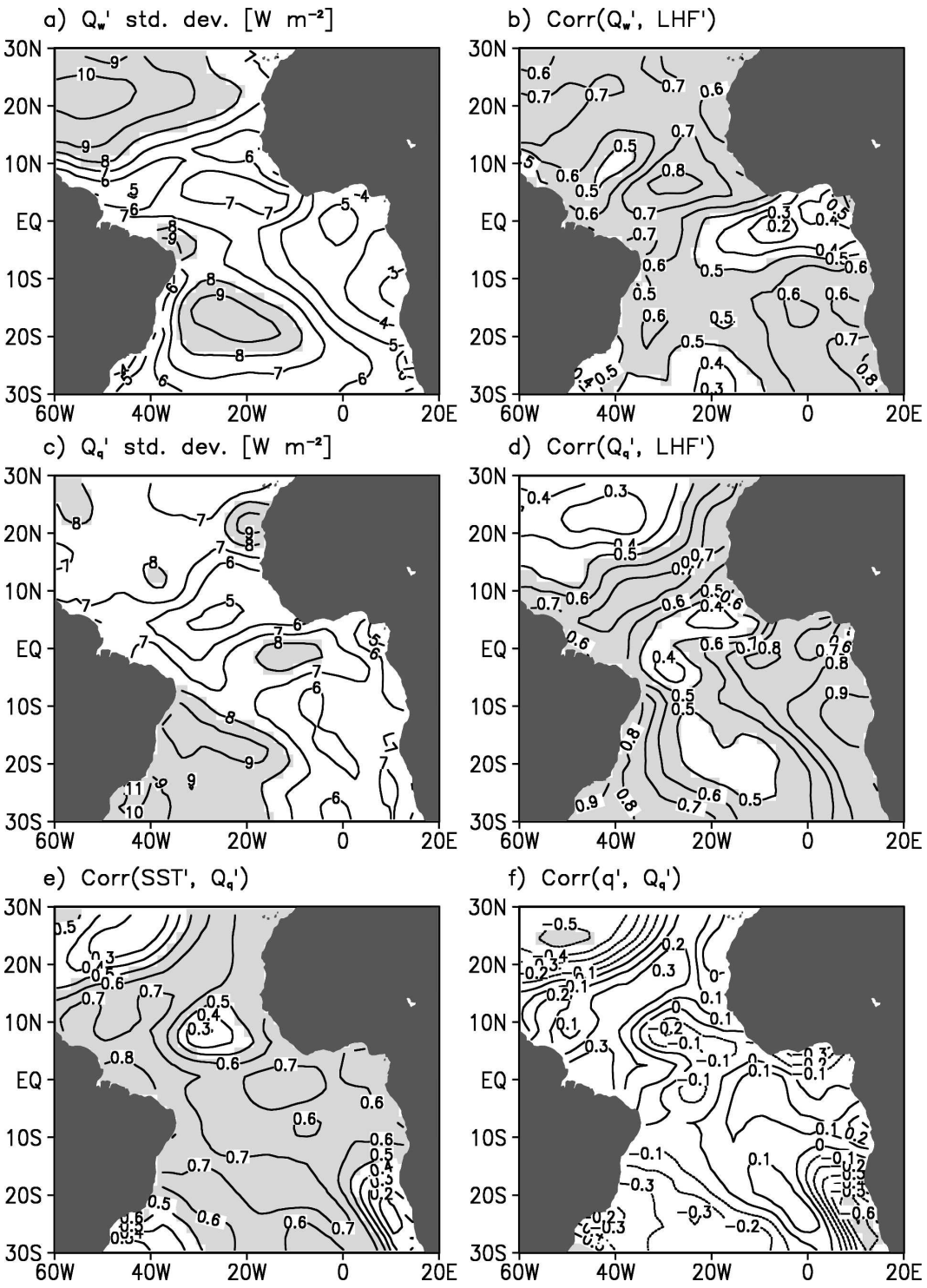

FIG. 5. (a) Interannual standard deviation of wind-induced LHF anomalies (Q'_w) and (b) correlation of total LHF anomalies (LHF') with Q'_w [see Eq. (3) and text for explanation]. (c) Interannual standard deviation of humidity-induced LHF anomalies (Q'_q) and (d) correlation of LHF' with Q'_q. Correlation of Q'_q with (e) SST' and (f) q'. Shading in (a) and (c) indicates regions of enhanced variability. Shading in (b), (d), (e), and (f) indicates where the magnitude of the correlation is >0.5.

TABLE 1. Zonal and meridional components of Ekman and geostrophic advection (shown as mean ± standard deviation in W m^{-2}), averaged in the tropical North Atlantic (10°–25°N, 20°–60°W) and in the tropical South Atlantic (5°–20°S, 30°W–10°E). Both means and standard deviations were computed during 1992–2002. Values >0 imply warming of the mixed layer [see (1)].

	10°–25°N	5°–20°S
$-(\rho c_p hu\partial T/\partial x)_{\mathrm{Ek}}$	−4 ± 2	−7 ± 3
$-(\rho c_p hu\partial T/\partial x)_{\mathrm{geo}}$	−1 ± 3	−3 ± 4
$-(\rho c_p hv\partial T/\partial y)_{\mathrm{Ek}}$	10 ± 4	12 ± 5
$-(\rho c_p hv\partial T/\partial y)_{\mathrm{geo}}$	−4 ± 4	−4 ± 4

reaches minima in the 10°–25° latitude bands of the western basin, where Q'_w dominates. These results are in agreement with previous studies, which indicate that wind-induced LHF drives SST variability throughout most of the tropical North and South Atlantic (Carton et al. 1996; Xie and Tanimoto 1998; Czaja et al. 2002).

5. Horizontal advection

In this section we examine the role of horizontal advection in the mixed layer heat balance. First, we compare the contributions from the Ekman and geostrophic components of advection. Averaged in the tropical North Atlantic (10°–25°N, 20°–60°W) and in the tropical South Atlantic (5°–20°S, 30°W–10°E) during 1992–2002, when sea level data are available, mean meridional Ekman advection induces warming of the mixed layer (Table 1). The warming is due to westward trade winds and their resultant poleward Ekman currents, combined with mean equatorward increasing SSTs (Figs. 1a,b). In contrast, the mean meridional geostrophic advection induces cooling that is weaker in magnitude and is caused by weaker mean equatorward currents acting on the meridional SST gradients. The mean zonal Ekman and geostrophic components of advection also induce weak cooling due to westward currents acting on westward increasing SSTs (Table 1).

Despite the dominance of meridional Ekman advection in the time mean, the variability of the Ekman and geostrophic components of advection is similar (Table 1). Everywhere poleward of 5°, however, anomalous heat advection by the geostrophic currents is poorly correlated with both local heat storage and the net surface heat flux (the absolute values of the correlations are <0.2 over the tropical Atlantic, with no spatially coherent patterns). This suggests that our estimates of geostrophic advection are mainly adding noise to the heat balance equation. The noisiness is likely a result of the small signal-to-noise ratio of the anomalous sea level data [the standard deviations of the sea level anomalies are <3 cm throughout the tropical Atlantic, in comparison to the measurement uncertainty of ~2 cm (Cheney et al. 1994)]. In contrast, in the 10°–20° latitude bands the Ekman advection is significantly correlated with the surface flux and local storage, as discussed later in this section. We therefore focus on the Ekman component of advection, which is available for a longer time period in comparison to geostrophic advection (1983–2002 versus 1992–2002). We note, however, that for the time period when sea level data are available, the results described in this section based on the Ekman currents are similar to the results obtained when the total currents are used.

In contrast to the net surface flux variability, which is fairly uniform at ~9–12 W m^{-2} throughout the tropical Atlantic (Fig. 3e), horizontal advection increases from a standard deviation of less than 3 W m^{-2} in the northern and southern Tropics to ~10 W m^{-2} equatorward of 10° (Fig. 6a). This equatorward increase can be explained by a corresponding equatorward increase in wind stress (Fig. 1b) and the f^{-1} dependence of the Ekman currents. In most of the tropical Atlantic, the standard deviation of meridional advection exceeds that of zonal advection (Figs. 6b,d), due mainly to stronger variability of the meridional SST gradient, which can be inferred from Fig. 2a. The only exceptions are in a meridional band within 10° of the African coast and in the zonal band of 5°–10°N, where the mean westward currents and the zonal SST gradient variability are strong.

Throughout most of the interior tropical Atlantic, horizontal advection acts as a negative feedback on the surface flux–driven heat storage variability (Fig. 7a). Here we define horizontal advection as $-\rho c_p h\nabla \cdot T$ so that a positive (negative) change in advection leads to a positive (negative) change in the mixed layer heat storage and a corresponding warming (cooling) of SST [see (1)]. Given our sign conventions for surface heat flux, negative correlations in Fig. 7a imply that as anomalous heat enters the mixed layer across the air–sea interface it is transported horizontally so as to reduce (damp) the original surface flux–induced SST anomaly. The strongest negative correlations between horizontal advection and the net surface heat flux are found in the central tropical South Atlantic and western tropical North Atlantic, a result of strong meridional advection that is partially counteracted by zonal advection (Figs. 7b,c).

To investigate the relevance of these advective heat fluxes to the interhemispheric SST gradient mode, we focus on two regions: one in the tropical North Atlantic (designated NATL: 10°–20°N, 30°–60°W) and one in the tropical South Atlantic (SATL: 10°–20°S, 5°–35°W) (Fig. 7a). These regions were chosen because they en-

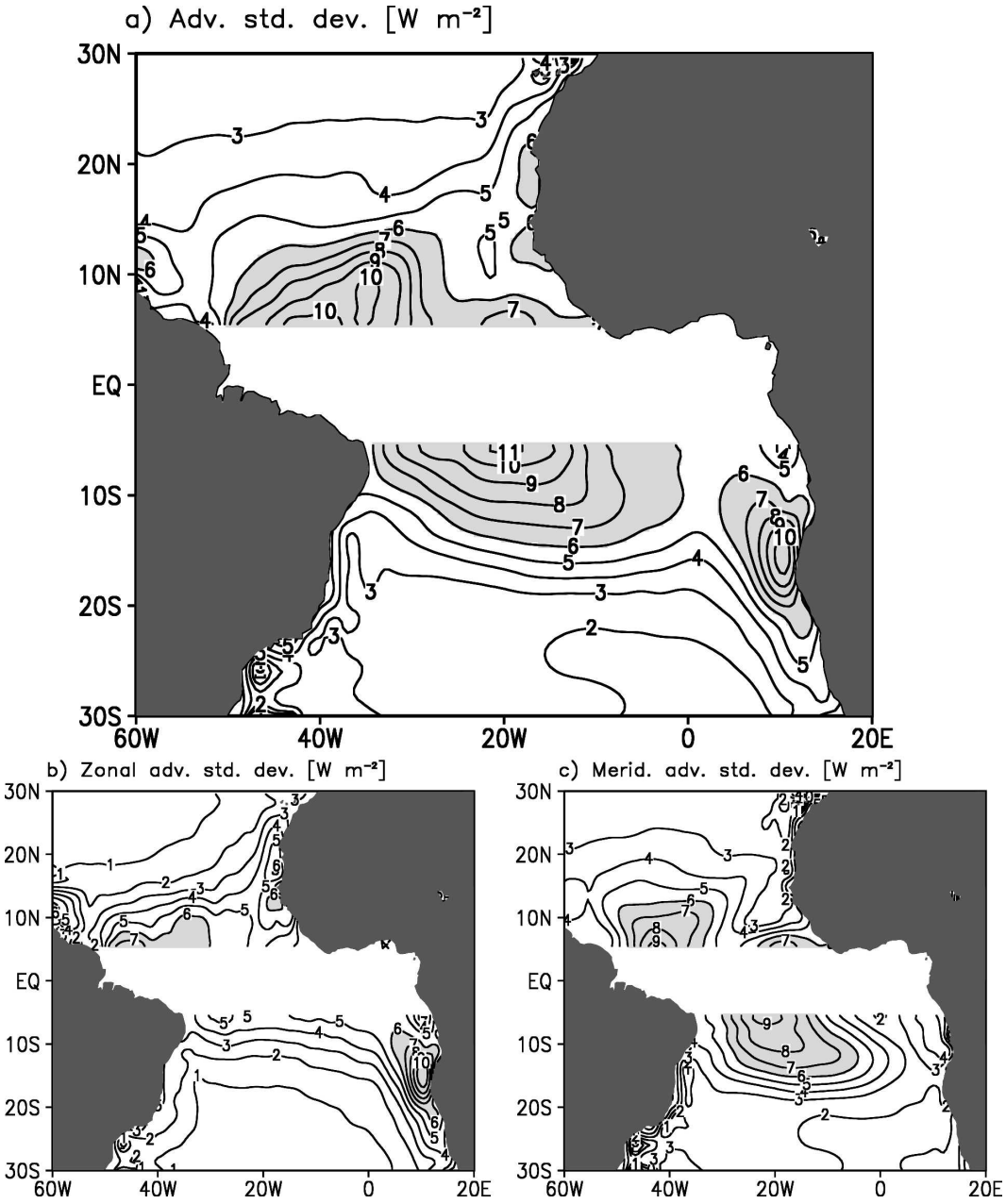

FIG. 6. Interannual standard deviation of (a) total horizontal mixed layer heat advection ($\rho c_p h \mathbf{v} \cdot \nabla T$), (b) zonal heat advection ($\rho c_p h u \partial T/\partial x$), and (c) meridional heat advection ($\rho c_p h v \partial T/\partial y$). Velocities are based on only the Ekman component of flow. Shading indicates regions of enhanced variability (>6 W m^{-2}).

compass the areas of strongest negative heat flux/advection correlations in each hemisphere and because they are representative of regions involved in the interhemispheric gradient mode in the tropical Atlantic. For this reason, they differ slightly from the regions used in the previous section. We define an interhemispheric SST index as the difference between SST averaged in the NATL region and SST averaged in SATL region. The index agrees well with Servain's (1991) dipole index, defined as SST in 5°–28°N, 20°–60°W minus SST in 20°S–5°N, 30°W–10°E (Fig. 8a). The correlation between the two is 0.9, indicating that the interhemispheric SST gradient variability is well represented by NATL and SATL SST differences. The regression of SST and surface winds onto our SST index reveals cross-equatorial winds in the western basin, with the strongest SST and surface wind variability located in the tropical North Atlantic (Fig. 8b). Both features are

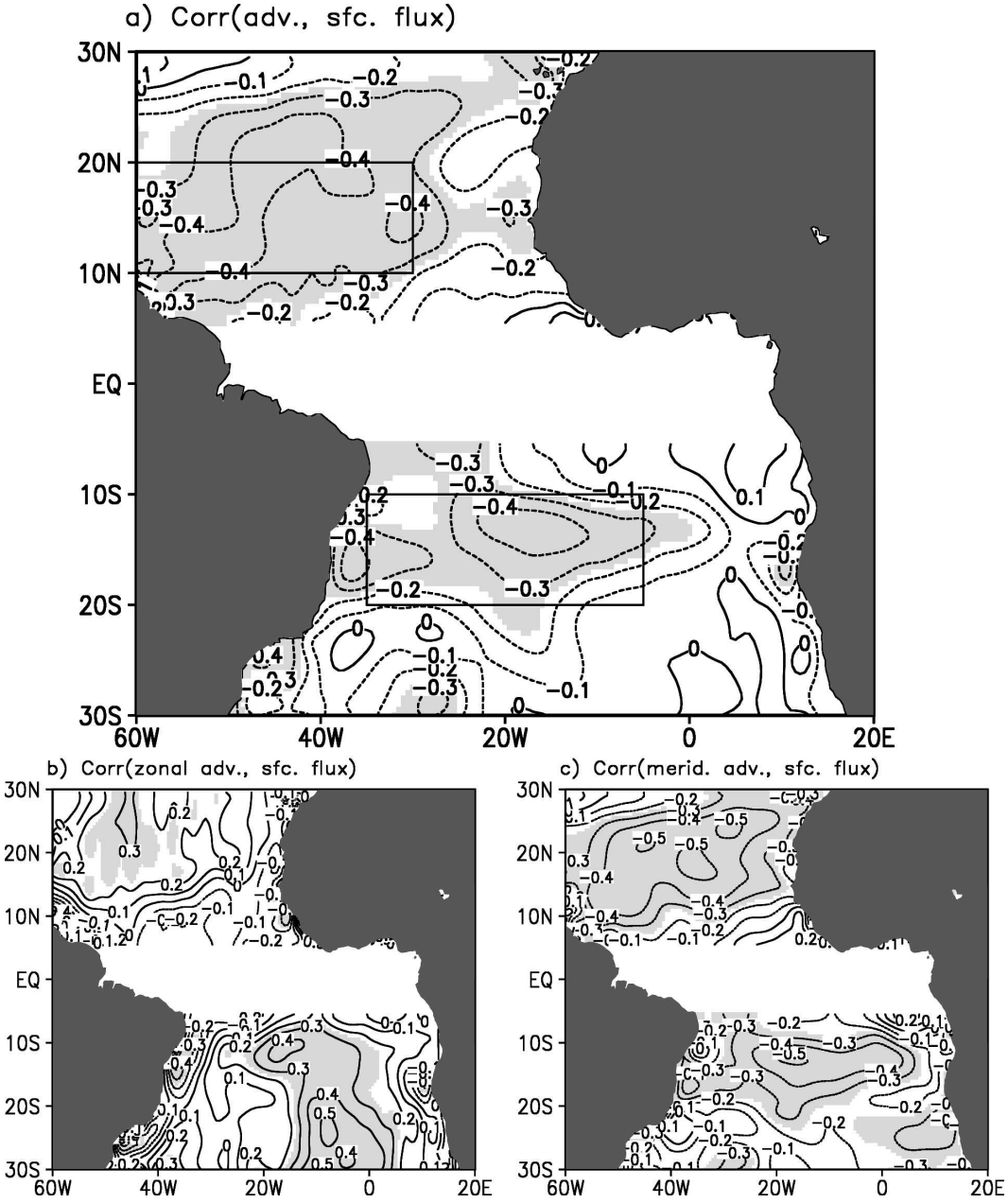

FIG. 7. Interannual anomaly correlation of the net surface heat flux with (a) total horizontal mixed layer heat advection, (b) zonal heat advection, and (c) meridional heat advection. Boxes enclose the regions used to form the NATL and SATL indices (Fig. 8). Shading indicates significance at the 10% level.

well-known characteristics of the interhemispheric SST gradient mode (Nobre and Shukla 1996; Chang et al. 2001).

In the SATL region both zonal and meridional advection are significantly correlated with the net surface heat flux (0.5 and −0.6, respectively) and the local storage (0.5 and −0.5, respectively), with standard deviations of 1 and 4 W m^{-2} for zonal advection and meridional advection, respectively (Fig. 9b). In the NATL region both zonal and meridional advection are similarly correlated with the surface flux (0.5 and −0.7, respectively) and local storage (0.4 and −0.5 respectively), but the variability of meridional advection is weaker than in the SATL region (standard deviations of 1 and 2 W m^{-2} for zonal and meridional, respectively; Fig. 9a).

In the NATL and SATL regions, meridional advection dominates zonal advection (Figs. 9a,b). The nega-

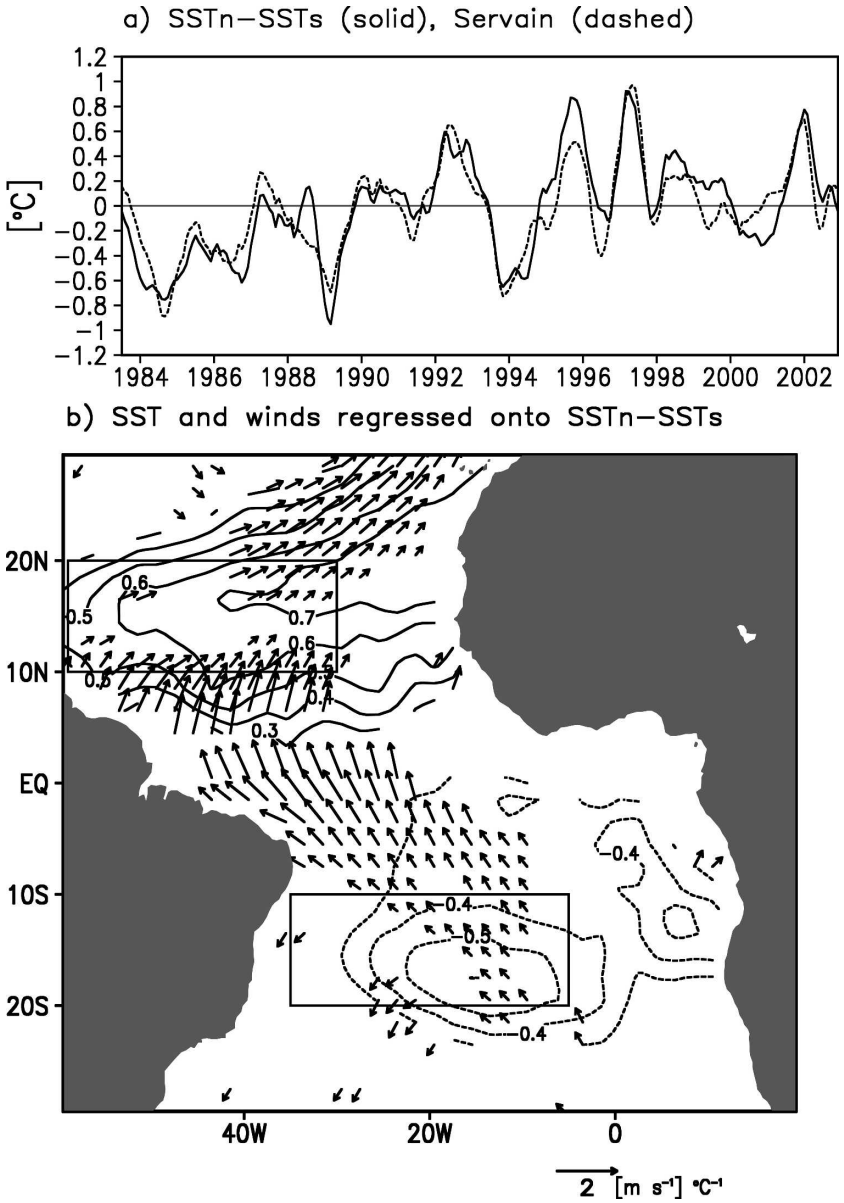

FIG. 8. (a) Anomalous interhemispheric SST gradient, defined as the SST anomaly averaged in the NATL region (SSTn: 10°–20°N, 30°–60°W) minus the SST anomaly averaged in the SATL region (SSTs: 10°–20°S, 5°–35°W) (solid) and Servain's (1991) index (dashed). (b) Anomalous SST and surface winds regressed onto SSTn–SSTs. Values are shown only where they are significant at the 10% level.

tive correlations between meridional advection and the net surface heat flux averaged in these regions can be explained by a combination of mean poleward Ekman currents acting on anomalous SST gradients (vT'_y) and anomalous currents acting on the mean equatorward SST gradient ($v'T_y$). In both regions, the two terms make comparable contributions as measured by their standard deviations. In the NATL region, the standard deviations of vT'_y and $v'T_y$ are both 1 W m^{-2}, while in the SATL region the standard deviations are 3 and 2 W m^{-2}, respectively. In both regions the two components are weakly but significantly correlated (0.3 for NATL and 0.4 for SATL).

Next, we investigate the causes of the significant positive correlations between the two meridional advection components in the SATL region. In this region, zonal wind stress (τ'_x) is significantly negatively correlated with T'_y, with the strongest correlation at zero lag

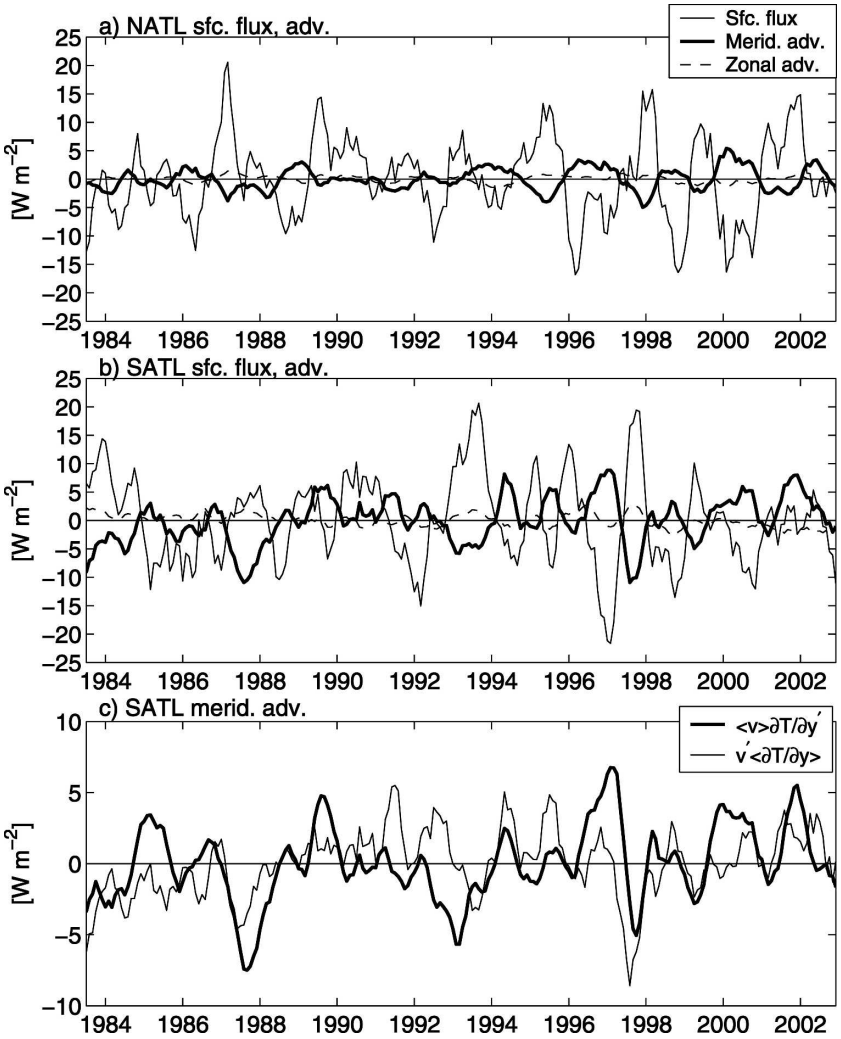

FIG. 9. Interannual anomalies of (a) net surface flux (thin solid), meridional advection (thick solid), and zonal advection (dashed) averaged in the NATL region. (b) Same as in (a), except for the SATL region. (c) Meridional advection components averaged in the SATL region: mean currents acting on anomalous SST gradients (thick) and anomalous currents acting on the mean SST gradient (thin). See Fig. 8 for definitions of NATL and SATL regions.

(Fig. 10a). The results are similar, but the correlations are of the opposite sign, when wind speed is used in the place of τ_x and also when $v'T_y$ and vT'_y are substituted for τ'_x and T'_y, respectively (Fig. 10a). This indicates that a westward (negative) wind stress (positive wind speed) anomaly is associated with an anomalously positive meridional SST gradient ($T'_y > 0$). The significant negative correlation between τ'_x and T'_y and the corresponding significant positive correlation between $v'T_y$ and vT'_y at zero lag cannot be explained simply in terms of the wind-induced LHF/SWR forcing of anomalous meridional SST gradients (vT'_y) and the associated wind stress forcing of anomalous meridional Ekman currents ($v'T_y$). If the wind were forcing T'_y and v', there would be a ~3-month lag between vT'_y and $v'T_y$ since the currents respond within an inertial period of ~1 day to the wind stress anomaly, while SST responds to the corresponding wind speed anomaly with a ~3-month lag (Fig. 10a). Instead, T'_y must be forcing τ'_x in the sense that an anomalous northward (southward) SST gradient leads to anomalous westward (eastward) wind stress. This assumption is supported by the results of Lindzen and Nigam (1987), which show that SST-forced surface pressure gradients in the Tropics force geostrophic surface winds outside of a few degrees of the equator.

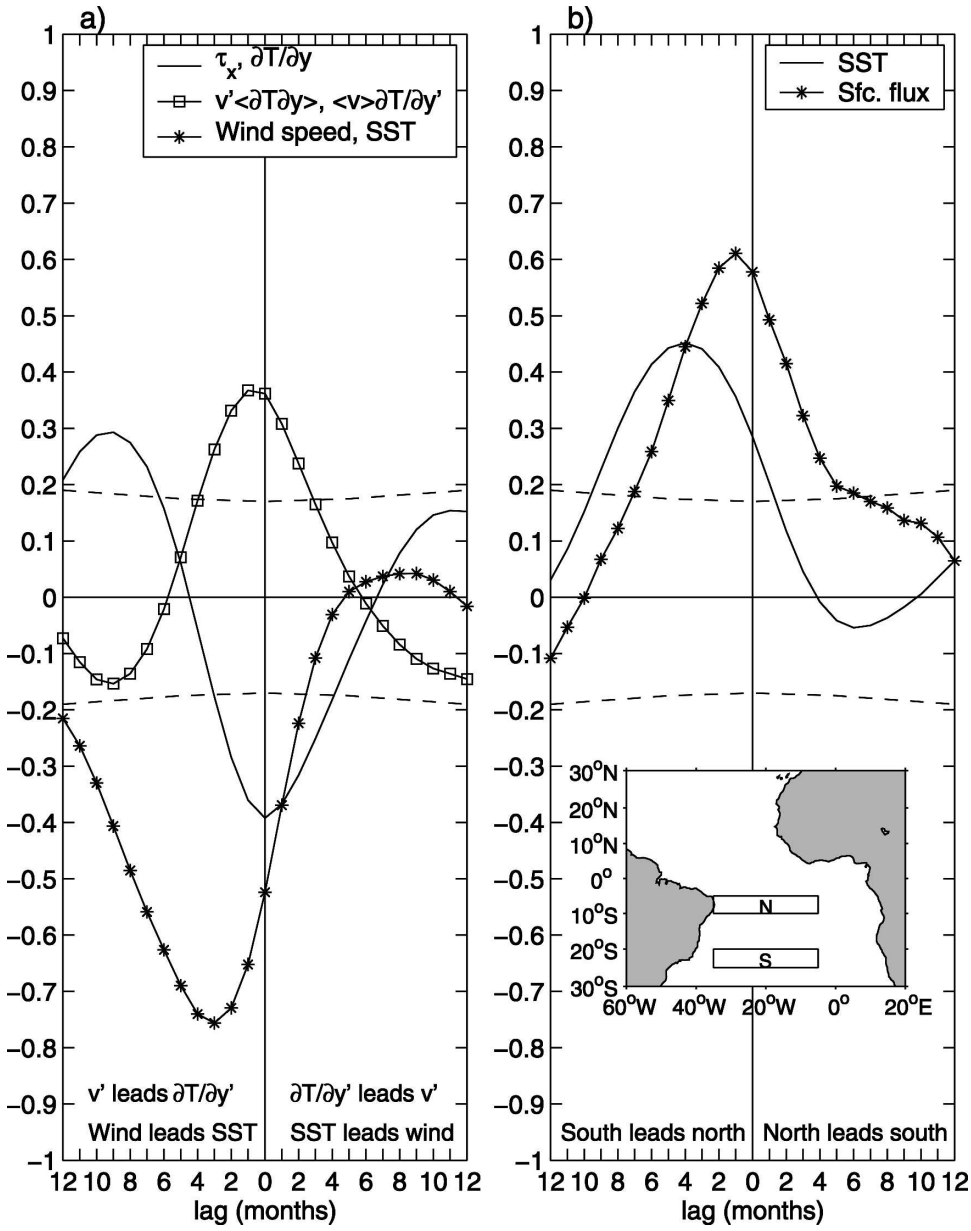

FIG. 10. (a) Lagged correlations between zonal wind stress (τ_x) and $\partial T/\partial y$ anomalies (solid), between $h\overline{v}'\overline{\partial T/\partial y}$ and $h\overline{v}\partial T/\partial y'$ (squares), and between wind speed and SST anomalies (asterisks), all averaged in the tropical South Atlantic (SATL: 10°–20°S, 5°–35°W). (b) Lagged correlations between SST anomalies averaged in the region south of the SATL region (20°–25°S, 5°–35°W) and SST anomalies averaged to the north of the SATL region (5°–10°S, 5°–35°W) (solid) and between the net surface flux averaged in the same regions (solid with asterisks). Map shows locations of the northern and southern regions used for averaging. Dashed lines indicate the 90% confidence levels for the correlations.

As a result of these coupled SST–$\partial T/\partial y$–wind speed interactions, initial SST and surface flux anomalies in the subtropical South Atlantic propagate northward as proposed by Xie (1999) and Huang and Shukla (2005; Fig. 10b). The ~3-month lag between SST in the southern and northern tropical South Atlantic (Fig. 10b) is also generally consistent with the results of Huang and Shukla (2005), who reported that SST signals propagate from the subtropical South Atlantic to the deep Tropics in about one season. We also find evidence for coupled interactions in the NATL region though the magnitude of variations in meridional advection is weaker than in the SATL region. In the NATL region, as in the SATL region, vT'_y and $v'T_y$ are significantly positively corre-

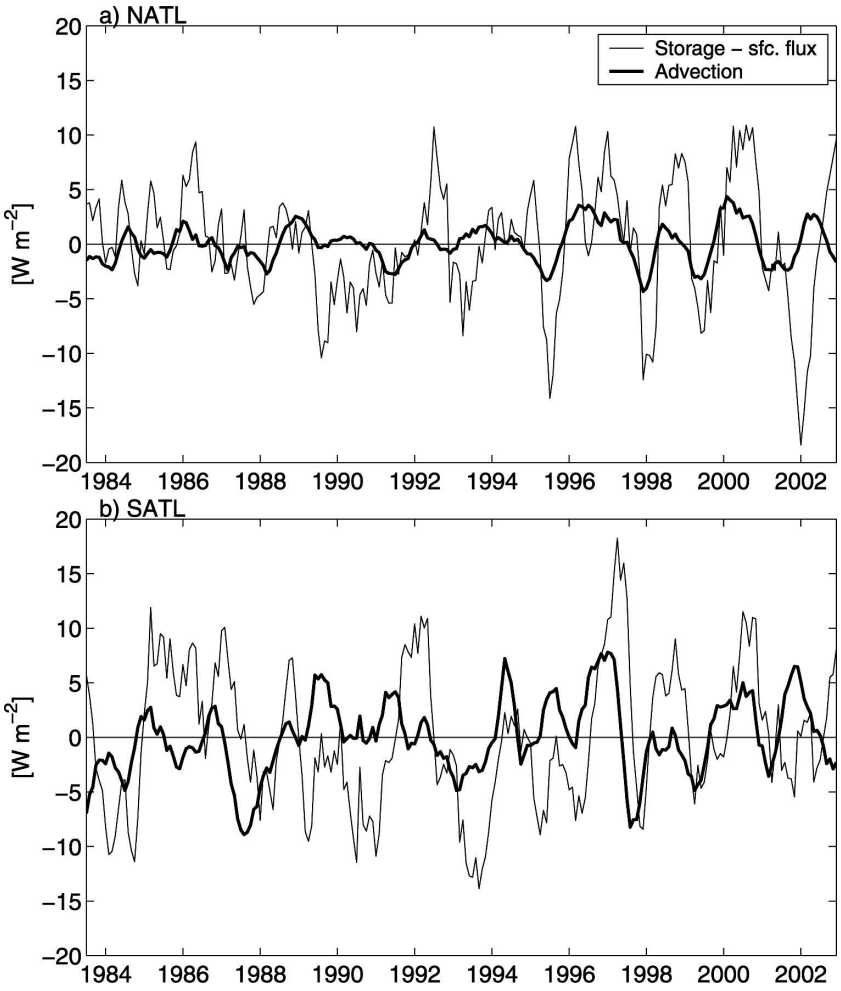

FIG. 11. (a) Difference between mixed layer heat storage and net surface heat flux (thin) and mixed layer horizontal heat advection (thick), averaged in the NATL region. (b) Same as in (a), except for SATL region (see Fig. 8 for definitions of NATL and SATL regions).

lated at zero lag, and there is a tendency for equatorward propagation of SST anomalies.

In the tropical North Atlantic and South Atlantic, the standard deviation of the net surface flux exceeds that of local storage by up to a factor of 2 (Figs. 2b, 3e, 4). Horizontal advection is of the correct sign to account for this discrepancy, providing a negative feedback on the local surface heat flux in the NATL and SATL regions. However, the strength of the horizontal advection is too weak to quantitatively explain the differences (Fig. 11). In the SATL region the standard deviation of the advection term is 50% of that of the storage/flux residual, while in the NATL region it is only 30%.

Possible explanations for the discrepancies include uncertainties in our estimation of surface fluxes, mixed layer currents, and mixed layer depth, as well as our neglect of entrainment and vertical turbulent diffusion. Our estimates of LHF are uncertain since they rely on a combination of satellite and reanalysis wind speed and humidity instead of direct measurements. The SWR estimates also contain uncertainty because they are not direct measurements, but instead use a combination of satellite-based cloud and aerosol concentrations and a radiative transfer model. There are uncertainties in our estimation of horizontal mixed layer heat advection due to our use of a model of the wind-forced currents and our neglect of geostrophic currents. Foltz and McPhaden (2005) found that, on intraseasonal time scales, the meridional Ekman currents in (2) significantly underestimated the true mixed layer currents, based on current meter data from the subduction buoy at 18°N, 34°W. It is also possible that entrainment and vertical diffusion may play important roles since, for example, positive (negative) anomalies of wind speed and wind stress curl may lead to positive (negative)

anomalies in turbulent vertical mixing and entrainment cooling. Finally, we are constrained by lack of data to use a climatological mean seasonal cycle for our estimates of mixed layer depth, which introduces additional uncertainty, especially in the tropical South Atlantic where the subsuface temperature and salinity data coverage is poor.

6. Summary and discussion

Through an analysis of the mixed layer heat balance, we have shown that variations of mixed layer heat storage in the tropical North and South Atlantic Ocean are driven primarily by latent heat loss and shortwave radiation. The role of horizontal oceanic heat advection in most of the tropical Atlantic is to damp the surface flux–forced changes in SST. The strongest damping occurs in the 10°–20° latitude bands of each hemisphere and is caused by a combination of the mean poleward Ekman currents acting on anomalous meridional SST gradients (vT'_y) and anomalous meridional Ekman currents acting on the mean equatorward temperature gradient ($v'T_y$). The two components are significantly correlated at zero lag as a result of coupled SST–$\partial T/\partial y$–wind interactions that originate in the subtropics. The coupled interactions are summarized as follows. A cold (warm) SST anomaly in the subtropical Atlantic sets up an anomalous equatorward (poleward) SST gradient on its equatorward side. The anomalous equatorward (poleward) SST gradient forces a westward (eastward) wind stress anomaly, which itself forces anomalous poleward (equatorward) Ekman currents, enhanced (reduced) wind-induced latent heat loss, and anomalously cold (warm) SST. Through these coupled interactions, the SST signal propagates equatorward and is damped by the combination of vT'_y and $v'T_y$.

In general, our results are similar to the theoretical results of Xie (1999) and the modeling-based results of Seager et al. (2001). Both found that SST in the tropical North and South Atlantic is driven mainly by surface heat fluxes and is damped considerably by horizontal advection. However, whereas Seager et al. (2001) and Chang et al. (2001) found the strongest damping equatorward of 10°, where the mean Ekman currents are the strongest, our results indicate that the regions of strongest damping are located farther poleward, generally in the 10°–20° latitude bands. Finally, Seager et al. (2001) showed that the contribution from vT'_y dominates $v'T_y$. However, our results indicate that $v'T_y$ is similar in magnitude to vT'_y in both the tropical North Atlantic and the tropical South Atlantic. This suggests a nontrivial role for $v'T_y$ in the heat balance, as hypothesized by Joyce et al. (2004). One possible reason for the differences between our analysis and that of Seager et al. (2001) is the difference in time scales considered. Seager et al. (2001) focused on decadal signals, while our results apply mainly to interannual signals due to the shortness of our records.

Despite the damping effect of horizontal advection in most of the tropical Atlantic, it is not strong enough to fully account for the stronger surface flux forcing in relation to the local storage. In both hemispheres the discrepancies are likely due to a combination of uncertainties in the estimation of latent heat flux, shortwave radiation, horizontal currents, and mixed layer depth. The planned addition of current meters at some Pilot Research Array in the Tropical Atlantic (PIRATA; Servain et al. 1998) sites will help to address uncertainties in our estimates of mixed layer currents. The growing database of temperature and salinity profiles from Argo floats, together with the planned enhancement of temperature and salinity measurements at some PIRATA sites, will help to improve estimates of mixed layer depth and heat storage. These new data, combined with continued improvements in the accuracy of surface flux products, will allow for more definitive assessments of the physical processes described in this paper. In the meantime, our results provide an empirical perspective on these processes that should be valuable in evaluating model simulations of tropical Atlantic climate variability.

Acknowledgments. We are grateful to Y. Zhang for providing the surface radiation dataset. We thank L. Yu for providing the turbulent heat flux dataset as well as the wind speed and specific humidity datasets used in the latent heat flux decomposition. We also thank two anonymous reviewers for their helpful suggestions. The NCEP–DOE reanalysis-2 data were provided by the NOAA Climate Diagnostics Center. This research was conducted while GF held a National Research Council Research Associateship Award at NOAA/PMEL.

REFERENCES

Carton, J. A., and B. H. Huang, 1994: Warm events in the tropical Atlantic. *J. Phys. Oceanogr.,* **24,** 888–903.

——, X. H. Cao, B. S. Giese, and A. M. daSilva, 1996: Decadal and interannual SST variability in the tropical Atlantic Ocean. *J. Phys. Oceanogr.,* **26,** 1165–1175.

Chang, P., L. Ji, and R. Saravanan, 2001: A hybrid coupled model study of tropical Atlantic variability. *J. Climate,* **14,** 361–390.

Cheney, R., L. Miller, R. Agreen, N. Doyle, and J. Lillibridge, 1994: TOPEX/Poseidon: The 2-cm solution. *J. Geophys. Res.,* **99,** 24 555–24 563.

Chikamoto, Y., and Y. Tanimoto, 2005: Role of specific humidity anomalies in Caribbean SST response to ENSO. *J. Meteor. Soc. Japan,* **83,** 959–975.

Czaja, A., P. Van der Vaart, and J. Marshall, 2002: A diagnostic study of the role of remote forcing in tropical Atlantic variability. *J. Climate,* **15,** 3280–3290.

de Boyer Montégut, C., G. Madec, A. S. Fischer, A. Lazar, and D. Iudicone, 2004: Mixed layer depth over the global ocean: An examination of profile data and a profile-based climatology. *J. Geophys. Res.,* **109,** C12003, doi:10.1029/2004JC002378.

Ducet, N., P. Y. Le Traon, and G. Reverdin, 2000: Global high-resolution mapping of ocean circulation from TOPEX/Poseidon and ERS-1 and -2. *J. Geophys. Res.,* **105,** 19 477–19 498.

Fairall, C. W., E. F. Bradley, J. E. Hare, A. A. Grachev, and J. B. Edson, 2003: Bulk parameterization of air–sea fluxes: Updates and verification for the COARE algorithm. *J. Climate,* **16,** 571–591.

Foltz, G. R., and M. J. McPhaden, 2005: Mixed layer heat balance on intraseasonal time scales in the northwestern tropical Atlantic Ocean. *J. Climate,* **18,** 4168–4184.

——, S. A. Grodsky, J. A. Carton, and M. J. McPhaden, 2003: Seasonal mixed layer heat budget of the tropical Atlantic Ocean. *J. Geophys. Res.,* **108,** 3146, doi:10.1029/2002JC001584.

Grodsky, S. A., and J. A. Carton, 2001: Intense surface currents in the tropical Pacific. *J. Geophys. Res.,* **106,** 16 673–16 684.

Hastenrath, S., and L. Greischar, 1993: Circulation mechanisms related to Northeast Brazil rainfall anomalies. *J. Geophys. Res.,* **98,** 5093–5102.

Huang, B. H., and J. Shukla, 2005: Ocean–atmosphere interactions in the tropical and subtropical Atlantic Ocean. *J. Climate,* **18,** 1652–1672.

——, P. S. Schopf, and J. Shukla, 2004: Intrinsic ocean–atmosphere variability of the tropical Atlantic Ocean. *J. Climate,* **17,** 2058–2077.

Joyce, T. M., C. Frankignoul, and J. Y. Yang, 2004: Ocean response and feedback to the SST dipole in the tropical Atlantic. *J. Phys. Oceanogr.,* **34,** 2525–2540.

Kanamitsu, M., W. Ebisuzaki, J. Woollen, S. K. Yang, J. J. Hnilo, M. Fiorino, and G. L. Potter, 2002: NCEP–DOE AMIP-II reanalysis (R-2). *Bull. Amer. Meteor. Soc.,* **83,** 1631–1643.

Klein, S. A., and D. L. Hartmann, 1993: The seasonal cycle of low stratiform clouds. *J. Climate,* **6,** 1587–1606.

Lagerloef, G. S. E., G. T. Mitchum, R. B. Lukas, and P. P. Niiler, 1999: Tropical Pacific near-surface currents estimated from altimeter, wind, and drifter data. *J. Geophys. Res.,* **104,** 23 313–23 326.

Lamb, P. J., 1978: Large-scale tropical Atlantic surface circulation patterns associated with sub-Saharan weather anomalies. *Tellus,* **30,** 240–251.

Lindzen, R. S., and S. Nigam, 1987: On the role of sea surface temperature gradients in forcing low-level winds and convergence in the tropics. *J. Atmos. Sci.,* **44,** 2418–2436.

Moisan, J. R., and P. P. Niiler, 1998: The seasonal heat budget of the North Pacific: Net heat flux and heat storage rates (1950–1990). *J. Phys. Oceanogr.,* **28,** 401–421.

Monterey, G. I., and S. Levitus, 1997: *Seasonal Variability of Mixed Layer Depth for the World Ocean.* NOAA Atlas NESDIS 14, 5 pp. and 87 figs.

Nobre, C., and J. Shukla, 1996: Variations of sea surface temperature, wind stress, and rainfall over the tropical Atlantic and South America. *J. Climate,* **9,** 2464–2479.

Reynolds, R. W., N. A. Rayner, T. M. Smith, D. C. Stokes, and W. Q. Wang, 2002: An improved in situ and satellite SST analysis for climate. *J. Climate,* **15,** 1609–1625.

Rio, M.-H., and F. Hernandez, 2004: A mean dynamic topography computed over the world ocean from altimetry, in situ measurements, and a geoid model. *J. Geophys. Res.,* **109,** C12032, doi:10.1029/2003JC002226.

Ruiz-Barradas, A., J. A. Carton, and S. Nigam, 2000: Structure of interannual-to-decadal climate variability in the tropical Atlantic sector. *J. Climate,* **13,** 3285–3297.

Seager, R., Y. Kushnir, P. Chang, N. Naik, J. Miller, and W. Hazeleger, 2001: Looking for the role of the ocean in tropical Atlantic decadal climate variability. *J. Climate,* **14,** 638–655.

Servain, J., 1991: Simple climatic indices for the tropical Atlantic Ocean and some applications. *J. Geophys. Res.,* **96,** 15 137–15 146.

——, A. J. Busalacchi, M. J. McPhaden, A. D. Moura, G. Reverdin, M. Vianna, and S. E. Zebiak, 1998: A Pilot Research Moored Array in the Tropical Atlantic (PIRATA). *Bull. Amer. Meteor. Soc.,* **79,** 2019–2031.

Simmons, A. J., and J. K. Gibson, 2000: The ERA-40 project plan. Tech. Rep., ECMWF, Reading, United Kingdom, 62 pp.

Sprintall, J., and M. Tomczak, 1992: Evidence of the barrier layer in the surface layer of the tropics. *J. Geophys. Res.,* **97,** 7305–7316.

Tanimoto, Y., and S. P. Xie, 2002: Inter-hemispheric decadal variations in SST, surface wind, heat flux, and cloud cover over the Atlantic Ocean. *J. Meteor. Soc. Japan,* **80,** 1199–1219.

Wang, W. M., and M. J. McPhaden, 1999: The surface-layer heat balance in the equatorial Pacific Ocean. Part I: Mean seasonal cycle. *J. Phys. Oceanogr.,* **29,** 1812–1831.

Wilks, D. S., 1995: *Statistical Methods in the Atmospheric Sciences.* Academic Press, 467 pp.

Xie, S.-P., 1999: A dynamic ocean–atmosphere model of the tropical Atlantic decadal variability. *J. Climate,* **12,** 64–70.

——, and Y. Tanimoto, 1998: A pan-Atlantic decadal climate oscillation. *Geophys. Res. Lett.,* **25,** 2185–2188.

Yu, L. S., R. A. Weller, and B. M. Sun, 2004: Improving latent and sensible heat flux estimates for the Atlantic Ocean (1988–99) by a synthesis approach. *J. Climate,* **17,** 373–393.

Zhang, Y., W. B. Rossow, A. A. Lacis, V. Oinas, and M. I. Mishchenko, 2004: Calculation of radiative fluxes from the surface to top of atmosphere based on ISCCP and other global data sets: Refinements of the radiative transfer model and the input data. *J. Geophys. Res.,* **109,** D19105, doi:10.1029/2003JD004457.